Environmental Science: Atmospheres

ROYAL SOCIETY OF CHEMISTRY

PAPER

View Article Online
View Journal | View Issue

Check for updates

Cite this: *Environ. Sci.: Atmos.*, 2024, **4**, 861

New airborne research facility observes sensitivity of cumulus cloud microphysical properties to aerosol regime over the great barrier reef†

Diana C. Hernandez-Jaramillo, *[a] Chris Medcraft,[a] Ramon Campos Braga,[a] Peter Butcherine,[a] Adrian Doss,[a] Brendan Kelaher,[a] Daniel Rosenfeld[b] and Daniel P. Harrison[a]

Our work on aerosol–cloud–radiation interactions became hamstrung by the lack of a suitable aerosol and cloud microphysics equipped aircraft in Australia. To address this infrastructure gap, we have established a new airborne research platform, designed primarily for Marine Cloud Brightening (MCB) field studies but with broader applicability across diverse airborne research domains. This platform, comprising a Cessna 337 aircraft was outfitted with a comprehensive suite of meteorological, aerosol, and cloud microphysical instrumentation normally only found on much larger aircrafts. The aircraft has completed its first field deployment over the Great Barrier Reef (GBR) supporting the Reef Restoration and Adaptation Program. Here we present details of the platform configuration, a flight summary of its first campaign and a case study illustrating the capabilities of the new platform. In the case study presented, data was collected from two well-developed cumulus cloud cells which were similar in macrophysical properties but formed under markedly different aerosol regimes. We observed a strong difference in cloud microphysical properties. Higher aerosol concentrations led to more numerous and smaller cloud drops and suppressed warm rain. Our observations are consistent with the hypothesis that cumulus clouds, dominant over the GBR during summer, are amenable to marine cloud brightening. Our results demonstrate the practical utility of the new research aircraft through a focused case study, laying the groundwork for future scientific investigations of aerosol–cloud interactions.

Received 19th January 2024
Accepted 25th June 2024

DOI: 10.1039/d4ea00009a

rsc.li/esatmospheres

Environmental significance

Understanding aerosol–cloud interactions is crucial for improving climate models and predictions of future scenarios, especially those involving solar radiation management techniques. Challenges associated with early stage of Marine Cloud Brightening field research, such as the measurement of shallow clouds and plume characterisation in remote areas over the Great Barrier Reef (GBR) led to the selection and modification of a novel airborne research facility for atmospheric studies. Key findings after the first aircraft deployment revealed the impact of continental pollution on the microphysical properties of marine clouds. The latter emphasises the vulnerability of pristine environments, such as the GBR, to anthropogenic influences. This study contributes to a broader comprehension of atmospheric processes, aiding in the formulation of sustainable environmental strategies to mitigate climate change impacts on delicate ecosystems, such as the GBR and beyond.

Introduction

Aerosol–cloud interactions play a significant role in the Earth's climate system.[1,2] Understanding how they influence cloud dynamics is critical to improving climate models and refining predictions of future scenarios,[3] especially those in which solar radiation management techniques are included.[4,5] Such understanding is important for establishing the efficacy of climate change adaptations, such as marine cloud brightening.[6,7]

Aerosol concentration, composition, and size distribution influence cloud microphysical properties, including reflectivity (albedo), and precipitation patterns. The first aerosol indirect effect, known as the Twomey effect,[8,9] shows that for a fixed liquid water path, increases in aerosols can increase cloud droplet concentration and, therefore, cloud albedo. The cooling impact resulting from changes in cloud albedo due to increases in cloud droplet concentration[10,11] led Latham[12] to suggest Marine Cloud Brightening (MCB) as a solar radiation management intervention. MCB aims to generate a cooling effect at the

[a]National Marine Science Centre, Southern Cross University, Coffs Harbour, 2450, Australia. E-mail: diana.hernandez@scu.edu.au

[b]The Hebrew University of Jerusalem, Institute of Earth Sciences, Jerusalem 91904, Israel

† Electronic supplementary information (ESI) available. See DOI: https://doi.org/10.1039/d4ea00009a

ocean surface by deliberately spraying sea-salt aerosols into the marine boundary layer, which in turn, increases the concentration of cloud condensation nuclei and cloud reflectivity.[6–9,13–20]

The potential of implementing MCB over regional areas[21,22] motivated the research under the Reef Restoration and Adaptation Program (RRAP) to reduce thermal stress over The Great Barrier Reef (GBR).[23–25] This intervention would target low-lying marine clouds under aerosol-limited regimes, specifically during the summer season[25] when extreme marine heatwaves can typically occur and trigger coral bleaching events.[26,27] An MCB spraying prototype has been tested during a series of summer field campaigns in the central region of the GBR from 2020 to 2022. The dispersion of the artificially generated plume of nano-sized sea-salt aerosols has been previously characterised by measuring total particle number concentration from remotely piloted aircraft systems.[28] These measurements up to 1 km distance from the source demonstrated that the evaporative cooling of the seawater droplets does not affect the nearfield dispersion of the plume as previously suggested by modelling studies.[29,30] Following these initial trials, the campaigns have escalated from one to two operating sprayers with 640 effervescent nozzles.[31–34] Measuring the efficacy of this more powerful spraying system required much greater spatial coverage of airborne measurements requiring aircraft with greater endurance, range and payload than the available remotely piloted aircraft.

Traditionally, research aircraft, especially those dedicated to cloud microphysics studies, have been predominantly jets or midsize aircraft designed to accommodate sophisticated scientific instrumentation at high altitudes and over long distances.[35–46] In contrast, field experimentation to explore Marine Cloud Brightening requires measurement of shallow clouds and plume characterisation within the atmospheric boundary layer. Early stage MCB field research will be conducted at limited spatial scales[7,47,48] and due to the dynamic dispersion of a plume from one or several point sources, sampling is ideally conducted at low airspeed to measure at higher spatial resolution (~40–50 m). Operations are required to be predominantly over ocean and potentially far from land, demanding aircraft mechanical reliability, redundancy, and ideally long flight endurance. Smaller twin engine light aircraft are well suited to this type of operation provided they can carry the required weight of instrumentation and personnel.

There are very few research aircrafts operated in Australia. They include two Diamond HK36TTC-ECO Dimonas operated by Airborne Research Australia (ARA) and a twin-engine Piper PA 44 Seminole operated by the University of New South Wales (UNSW). The Dimona aircrafts are single-engine motor gliders that have been previously equipped with meteorological and remote sensing equipment. They have the capability for aerosols measurements[49,50] but are not certified to perform flights within cloud restricting the operation of cloud microphysics instruments. The Piper PA 44 Seminole is equipped for aerial lidar and photography survey operations such as for beach erosion[51,52] and bushfire recovery.[53] While this aircraft could be equipped with instrumentation for aerosol and cloud microphysical studies its payload and endurance are quite limited for this aircraft class.

An analysis of MCB operational requirements led to the selection and development of a Cessna 337G Skymaster. The outfitting of this aircraft and the required modifications to integrate a comprehensive suite of meteorological, aerosol, and cloud microphysics instrumentation is described in the first section of this manuscript, followed by an example of *in situ* measurements obtained during its first deployment in the RRAP Cooling and Shading Campaign (Mar–Apr 2023). Results presented were obtained from precipitating cumulus clouds formed in clean and polluted conditions over the GBR. Our findings show the effect of continental pollution on microphysical properties of marine clouds, typically formed in clean conditions. We show that marine clouds over the GBR develop as polluted due to the long-range transport of aerosol particles from the east coast of Australia. In such scenario, a larger number of droplets activated at cloud bases and above, leading to warm rain suppression and the increasing of height of warm rain initiation. This paper is intended as a point of reference for future detailed scientific publications presenting results from the cooling and shading campaign Mar–Apr 2023.

Aircraft characteristic and modifications

The Cessna 337G Skymaster is a push–pull twin engine aircraft with capacity for up to 5 passengers and a pilot (see Table 1 for general technical specifications). The IO-360 Continental engines are unusually arranged with one at the front of the fuselage and one at the rear, providing redundancy with the increased safety of no asymmetric thrust in the case of an engine failure. This unique safety feature is especially valuable when flying low and slow, a flight condition often desired in research operations. The front-rear engine layout combined with the high-wing configuration, allows for installation of instruments under the wings away from the influence of the propeller and exhaust wash. With a top cruise speed of 86.9 m s^{-1} (169 kts) and stall speed of 31.4 m s^{-1} (61 kts), the Cessna 337 offers a stable low speed platform suitable for high

Table 1 Technical specification of Cessna 337G Skymaster when outfitted with aerosol and cloud physics instrumentation and at max take-off weight[a]

Cessna 337G skymaster characteristics	
Max take-off weight	4630 lb (2100 kg)
Max speed	89 m s^{-1} (173 kts)
Cruise speed	86.9 m s^{-1} (140 kts)
Stall speed	31.4 m s^{-1} (61 kts)
Sampling speed	46.3–72 m s^{-1} (90–140 kts)
Max endurance	6.9 hours
Typical rate of climb at sea level	3.8 m s^{-1} (750 fpm)
Ceiling*	5.5 km (18 000 ft)

[a] Manufacturer provided figures which have not been retested to account for the additional drag of the instrumentation are marked with *.

resolution mapping of aerosol or cloud microphysical properties in limited spatial extents. Additionally, the aircraft is certified to operate by Instrument Flight Rules (IFR), which allow missions in poor visibility conditions such as rain, within cloud, fog or at night. Aircraft endurance allowed us to conduct flight missions of up to 6 hours flying at ~46.3–51.4 m s^{-1} (~90–100 kts) while maintaining fuel reserves required by IFR operations.

Modifications to the aircraft were intended to accommodate relevant scientific instrumentation for aerosol, meteorological and cloud properties measurements. Alterations of the aircraft cabin included removing the rear row passenger seats and one centre row seat for the installation of a four-level rack that holds the main data collection computer and majority of the aerosol instrumentation. External modifications include an aerodynamic pod that was fabricated from carbon fibre and was mounted to existing fuel drop-tank hard points under the right hand (RH) wing. This pod served to house the aerosol inlet, drying system, optical particle sizer, and dewpoint mirror. It was designed to flexibly accommodate additional instrumentation in the future. Hard points under the left hand (LH) wing were used to carry the DMT Cloud Combination Probe (CCP) using a custom-made pylon. Structural changes were also required outboard each wing to mount an ARIM 200 air data probe from Aventech on the LH wing and a net radiometer from Apogee on the RH wing. Four Milesight network cameras were installed in different parts of the aircraft to record flights (one looking upward on top of the fuselage, one on the pod looking forward, two under the RH wing – looking downward and forward). Fig. 1 shows the final configuration of the major external instrumentation, which will be described in more detail in the following section.

Instrumentation

Scientific instrumentation was divided into five systems which include measuring aerosol, radiation, cloud properties, meteorological conditions and aircraft position and attitude. A power distribution and a data processing system were also added to integrate all the scientific equipment into the aircraft (Table S1 in ESI† shows a summary of the instrumentation used on each system).

Aerosol instrumentation system

The aerosol system was divided between two locations (Fig. 2). From the underwing pod undisturbed air is sampled through an isokinetic inlet. The inlet body was developed by Airborne Research Australia and was improved by addition of an Arduino microcomputer which processes velocity and pressure information from the ARIM200 sensor to maintain isokinetic conditions at the intake. Immediately downstream of the inlet, a three-way valve (Brechtel, USA) was installed to be able to

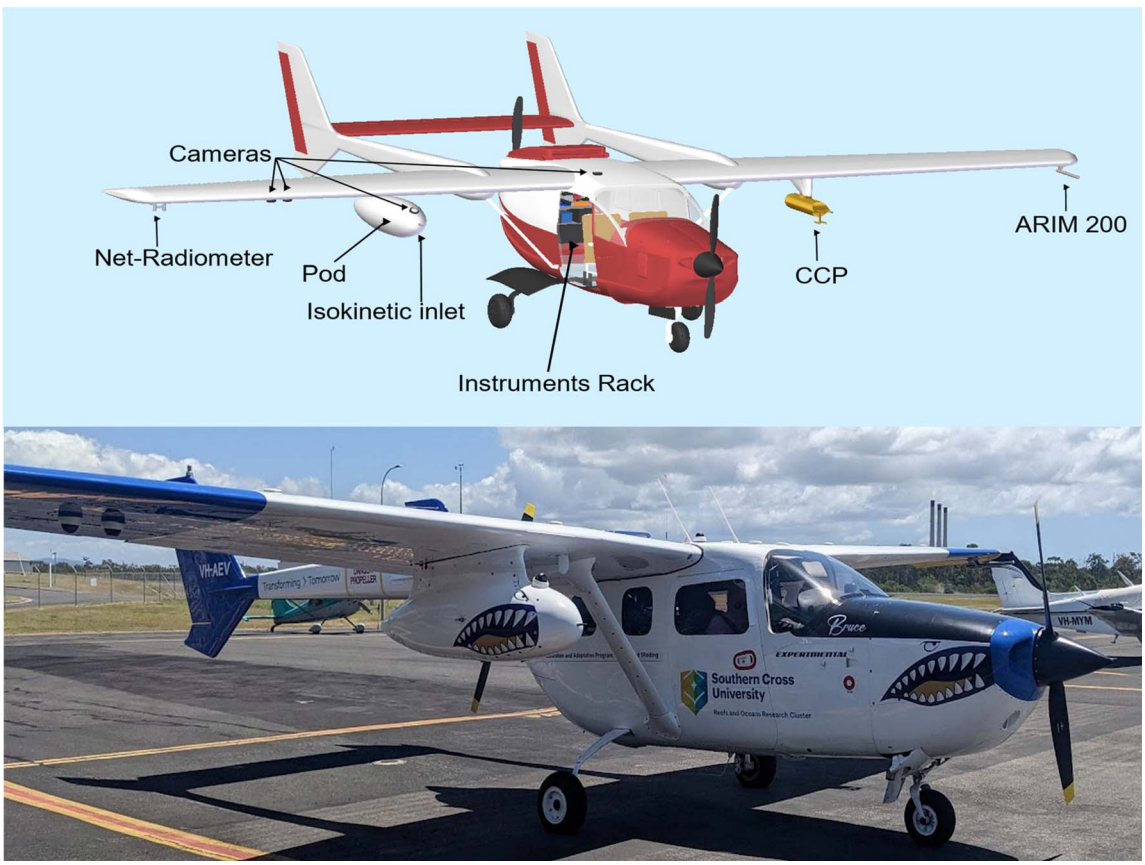

Fig. 1 Conceptual design of the aircraft sampling platform showing major external instrumentation and photo of the final configuration.

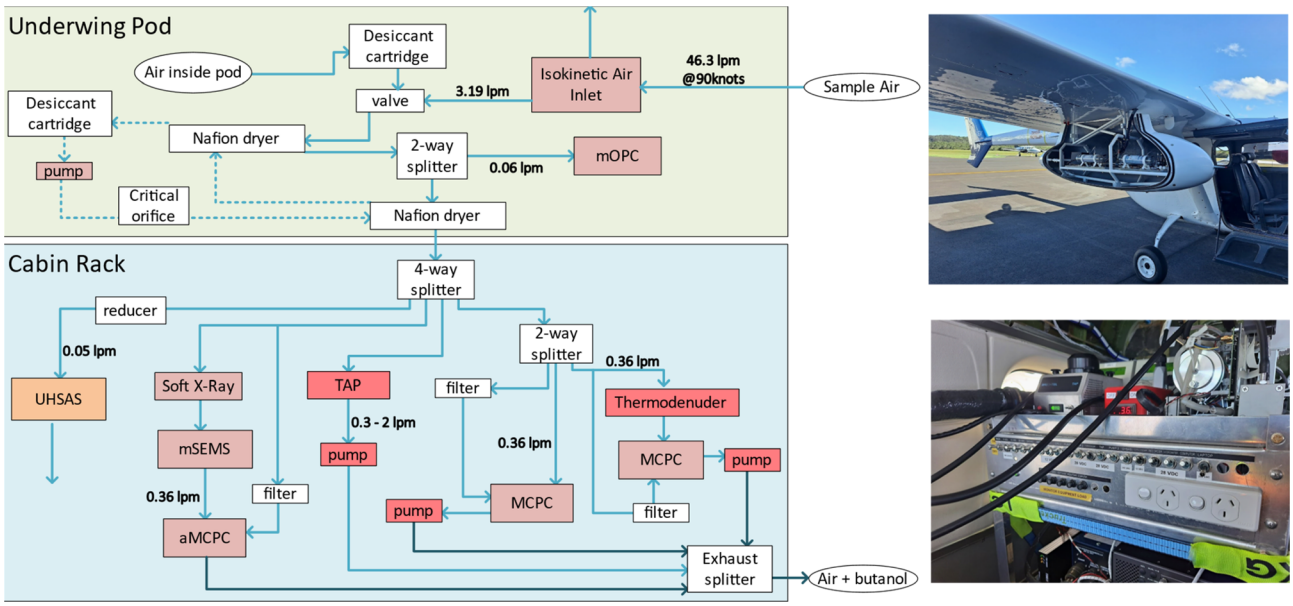

Fig. 2 Flow diagram of the aerosol instrumentation accessing sample air from the isokinetic inlet in the underwing pod, and cabin. Flow rate requirements of the system is presented in litre per minute (lpm). Photos taken from the underwing pod installed on the Cessna 337 and the cabin rack.

switch between sample air and desiccant dried air from inside the pod in cases where relative humidity (due to rain, in-cloud measurements or drying system failure) exceeded the limit required for the instruments. The sampled air then passes through a Nafion dryer after which it is split. Part of the flow continues to a miniaturised Optical Particle Counter (9405 mOPC; Brechtel, USA) mounted in the pod. The mOPC performs particle number size distribution measurements at 1 Hz over a particle diameter range between 190 and 3000 nm. The arrangement of the inlet, valve, Nafion dryer and mOPC is such that sample air reaching the mOPC travels in a near straight line over a distance of less than 1 m before being sampled. This arrangement was designed to minimise sampling losses for larger aerosols measured by the mOPC, specifically sea salt aerosol. The concentration range of the mOPC is 0 to 50 000 cm^{-3} with <10% error.

The remainder of sample air passes through a second Nafion dryer then through conductive tubing to the cabin where it is split amongst the instruments inside the fuselage. For the purpose of accurately sizing dry aerosol particles the relative humidity of the sample air was monitored at multiple locations throughout the system including, at the inlet of the mOPC (after the first Nafion dryer), after the second Nafion dryer before transport to the aircraft cabin, and finally at the inlet of the mSEMS (taken as being representative of sample line relative humidity for all cabin instruments).

The remaining aerosol sizing equipment includes an Ultra-High Sensitivity Aerosol Spectrometer (UHSAS; Droplet Measurement Technologies, USA) which is an optical-scattering, laser-based (λ = 1054 nm) aerosol particle spectrometer for sizing particles from 0.06 to 1 μm. Since it was the heaviest instrument, it was located on the bottom shelf of the rack and it set the minimum dimensions of the rack. Before the aircraft campaign, the UHSAS was calibrated with monodisperse polystyrene latex spheres of known size at DMT (Droplet Measurement Technologies, USA). Typical uncertainties of UHSAS measurements are 15% in diameter and concentration.[54,55]

The final aerosol sizing instrument is a miniaturized Scanning Electrical Mobility Sizer (9404 mSEMS; Brechtel, USA) which was coupled to an advanced Mixing Condensation Particle Counter (9403 aMCPC; Brechtel, USA). The mSEMS is a fast-electrical mobility-based particle sizer that provides size distribution of particles from 5 to 375 nm, but for this campaign it was set between 10 and 150 nm to provide higher time resolution in the size spectra below the UHSAS. The aMCPC performs ultra-fast total particle number concentrations up to 100 000 cm^{-3} with an uncertainty of ±8%.

Further aerosol instrumentation includes a 3-wavelength tricolor absorption photometer (TAP; Brechtel, USA) used for black carbon measurements at wavelengths of 467, 528 and 362 nm and noise of ±0.2 Mm^{-1} (0.02 μg m^{-3} black carbon mass).[56,57] Two mixing condensation particle counters (1720 MCPC; Brechtel, USA) were included in addition to the unit forming part of the mSEMS. These particle counters are able to detect particles between 7 and 2000 nm with a response time of 180 milliseconds and a coincidence corrected concentration uncertainty at 100 000 cm^{-3} of ±8%.[58] One of the MCPC measures total particle concentration and the other received sample air pre-treated using a thermodenuder (Flexotherm Industrial Heated Sample Line; Neptech, USA) set to 300 °C to determine the concentration of non-volatile particles. The ratio of volatile to non-volatile aerosol is intended to aid in identification of the MCB sea-salt aerosol plume. All Brechtel

instrumentation was recalibrated by the manufacturer immediately prior to the campaign. Three diaphragm pumps (7006VD/2,3/E/BLDC; Thomas, USA) were installed to supply the required sample flow for the TAP (0.3–2 lpm) and the two MCPCs (0.36 lpm each).

Cloud microphysics instrumentation

A Cloud Combination Probe (CCP) from DMT (Droplet Measurement Technologies, USA) was mounted under the LH wing (Fig. 3). The CCP combines three individual instruments, a Cloud Droplet Probe (CCP–CDP), a grayscale Cloud Imaging Probe (CIPg), and a hotwire liquid water sensor (LWC). The CDP counts the number of cloud particles and determines their individual size (detection range 3–50 μm) from the intensity of the forward-scattered laser light. Larger particles from 15 μm to 960 μm are detected by the CIPgs, and the particle sizes are reconstructed from 2D shadow images using the shadowgraph technique.[59] In addition, the liquid water content of clouds was measured by a King hot-wire probe[60] installed in the CCP. The CCP–CDP was calibrated with monodisperse glass beads spheres of known size at DMT. The CCP–CIPgs were also calibrated using a spinning disk by DMT immediately prior to the campaign. Calibration of the CDP was checked daily during the campaign using monodisperse glass beads.

The uncertainties in particle sizing of CCP–CDP measurements have shown uncertainties smaller than 10% during the campaign. Similar low uncertainty was found for the liquid water content estimated by the mass of the drops integrated over the diameter range of 3–50 μm and measured by a King probe-type device mounted on the CCP. During the campaign, measurements with the spinning disk calibration tool from DMT were done on regular bases to check functionality and a consistent resolution of the CIP.

A Cloud Condensation Nuclei counter (CCNc) from DMT (Droplet Measurement Technologies, USA), was provided for in the aircraft fit-out. This instrument counts the number of particles that activate into cloud droplets at a programmed supersaturation, or range of supersaturations. It was not included in the final configuration of the aircraft for this campaign. The fieldwork was conducted within a limited spatial region supported by a surface-based laboratory on Heron Island continuously sampling the atmospheric boundary layer. It was considered more advantageous to operate the instrument within this laboratory where it could continuously sample the atmospheric boundary layer while scanning through multiple supersaturations. The CCNC was operated at the laboratory in conjunction with an aerosol mass spectrometer, a proton transfer mass spectrometer, and aerosol sizing and concentration instrumentation.

Fig. 3 Photo of left-hand underwing probes showing the mounting of the Cloud Combination Probe (CCP) from Droplet Measurement Technologies (DMT) and the ARIM200 Air Data Probe (ADP) from Aventech.

Meteorology instrumentation

The ARIM200 air data probe (Aventech, USA) is an air-data sensing system that provides accurate GPS, inertial rates, air-data and meteorological data including barometric (static) pressure, air speed (including true airspeed (TAS)), angle-of-attack (AOA), angle-of-sideslip (AOS), outside air temperature (OAT), and relative humidity (%RH). The system includes an Air Data Probe (ADP) externally mounted on the outboard LH wing (Fig. 3), a high-accuracy three-dimensional differential GPS aided inertial measurement unit hard-mounted on the roof inside the cabin, two GPS antennas mounted one on each wing, and, a Touch Screen Display Module running Aventech MetTrack Firmware installed in the aircraft cockpit. The respective estimated uncertainties for temperature, relative humidity, and three-dimensional wind speed measurements are 0.3 °C, 2%, and 0.5 m s^{-1}.

A sensor unit for the 1011C Dew Point Hygrometer system (Buck Research Instruments, USA) was installed in the underwing pod, while its control unit was housed in the cabin instrument rack. This chilled mirror optical dew point system is capable of measuring dew and frost point temperatures between −75° and 50 °C.

Radiation instrumentation

The SN-500-SS Apogee Net Radiometer is a four-component instrument, with Individual upward and downward-looking blackbody pyranometers to measure shortwave radiation (0 to 2000 W m^{-2}) and pyrgeometers pairs to measure longwave radiation (−200 to 200 W m^{-2}). It was installed on the RH wing tip and data was collected using a dedicated datalogger mounted in the rack (CR1000X; Campbell Scientific, USA).

Data processing, storage, & display

Data processing and storage for most of the equipment was achieved using an ATC 8110 computer. A monitor was mounted for the instrument operator to display and control data collection during flight. Additionally, a GPS network time server (TM1000AGPS; TimeMachines, USA) was also integrated to synchronise time across all networked instruments and systems.

Power supply and distribution system

The two aircraft alternators were upgraded from 37 to 70 Amp to satisfy power requirements. In addition, a 240 V inverter, a 12 V and a 5 V transformer were added to the cabin rack to provide correct voltages to the various instruments and systems integrated into the aircraft. A power distribution panel was added within the fuselage to distribute power to the wing mounted systems, and a second panel on the rack to power equipment within the cabin.

Field campaign

The RRAP Cooling and Shading 2023 summer field campaign was conducted from March to April in the vicinity of Heron Reef (23.44°S, 151.88°E). The objectives of the campaign were to characterise existing aerosol–cloud interactions over the GBR during summer, examine the susceptibility of clouds to MCB perturbation, and test the viability of shading corals with an artificially generated sea-spray fog. Throughout the campaign, a total of 26 research flights (as shown in Table 2) were conducted exclusively during daylight hours. This region of the GBR is situated around 80 km offshore from the coastal city of Gladstone (23.84°S, 151.26°E), Australia, where the airport facility was located.

Here, we show two case studies of aerosol and cloud data collected in clean and polluted conditions in the lower troposphere. The background vertical profiles of aerosols and clouds microstructure (outside any influence of spraying operations) were sampled by performing cross-section transects at different altitudes inside two well developed clouds.

A general flight strategy during the campaign is described at Section S2 in the ESI.† Here we describe the parts relevant to the background cloud and aerosol data presented. The flights consisted of a low-level leg from the coast to the experimental site, monitoring background boundary layer conditions in an inshore-offshore transect. In proximity of the site a vertical profile was collected by spiral ascent to 3 km (10 000 ft) upwind of the vessel to avoid any influence of spraying operations. Followed by in-cloud cross-sections documenting background clouds.

Clean and polluted warm clouds over the GBR

We present the comparison of two well developed cumulus clouds as an illustrative example of the new airborne research platform capabilities. Fig. S2 in the ESI† includes scene classification of cloud type from satellite remote sensed data and stills retrieved form the aircraft camera for context of the type of clouds sampled. The first case was obtained during a flight on

Table 2 Summary of flights performed during the RRAP cooling and shading campaign 2023[a]

Flight ID	Date	Flight time (h)	Mission	Flight strategy
20230304	4/03/23	1.7	Test	Cloud passes
20230305	5/03/23	2.4	MCB	Cloud passes
20230307	7/03/23	3.1	MCB	Cloud passes
20230308	8/03/23	4.1	MCB	Plume mapping*
20230309	9/03/23	5.2	MCB control	Plume mapping*
20230312	12/03/23	4.1	Fogging	Plume mapping
20230313	13/03/23	2.6	MCB	Plume mapping*
20230314	14/03/23	3.8	MCB	Plume mapping*
20230315	15/03/23	4.3	MCB control, fogging	Plume mapping*
20230316	16/03/23	5.6	MCB	Plume mapping*
20230320	20/03/23	4.5	MCB	Cloud passes
20230321	21/03/23	4.9	MCB	Cloud passes
20230322	22/03/23	5.6	MCB	Cloud passes
20230323	23/03/23	4.5	MCB	Cloud passes
20230325_F1	25/03/23	5.5	MCB	Cloud passes*
20230325_F2	25/03/23	3.3	Fogging	Cloud passes*
20230326	26/03/23	5.2	MCB	Cloud passes*
20230327	27/03/23	5.8	MCB	Cloud passes*
20230328_F1	28/03/23	3.7	Fogging	Cloud passes*
20230328_F2	28/03/23	3.8	Fogging	Cloud passes*
20230329	29/03/23	5.7	Fogging	Cloud passes*
20230330	30/03/23	4.6	MCB	Cloud passes*
20230331	31/03/23	4.6	MCB control	Plume mapping and cloud passes*
20230401	1/04/23	5.2	MCB	Cloud passes*
20230404_F1	4/04/23	5.1	MCB	Cloud passes*
20230404_F2	4/04/23	3.4	MCB control	Plume mapping*

[a] The validity of the cloud and aerosol data collected during each flight is marked with *. Plume mapping refers to strategies to track the dispersion of the marine cloud brightening (MCB) plume. Cloud passes refers to in-cloud transects at several heights. MCB control refers to measurements of the emissions from the exhaust of the generator on the spraying boat. Fogging refers to an alternative cooling and shading technique of localised marine fog generation.

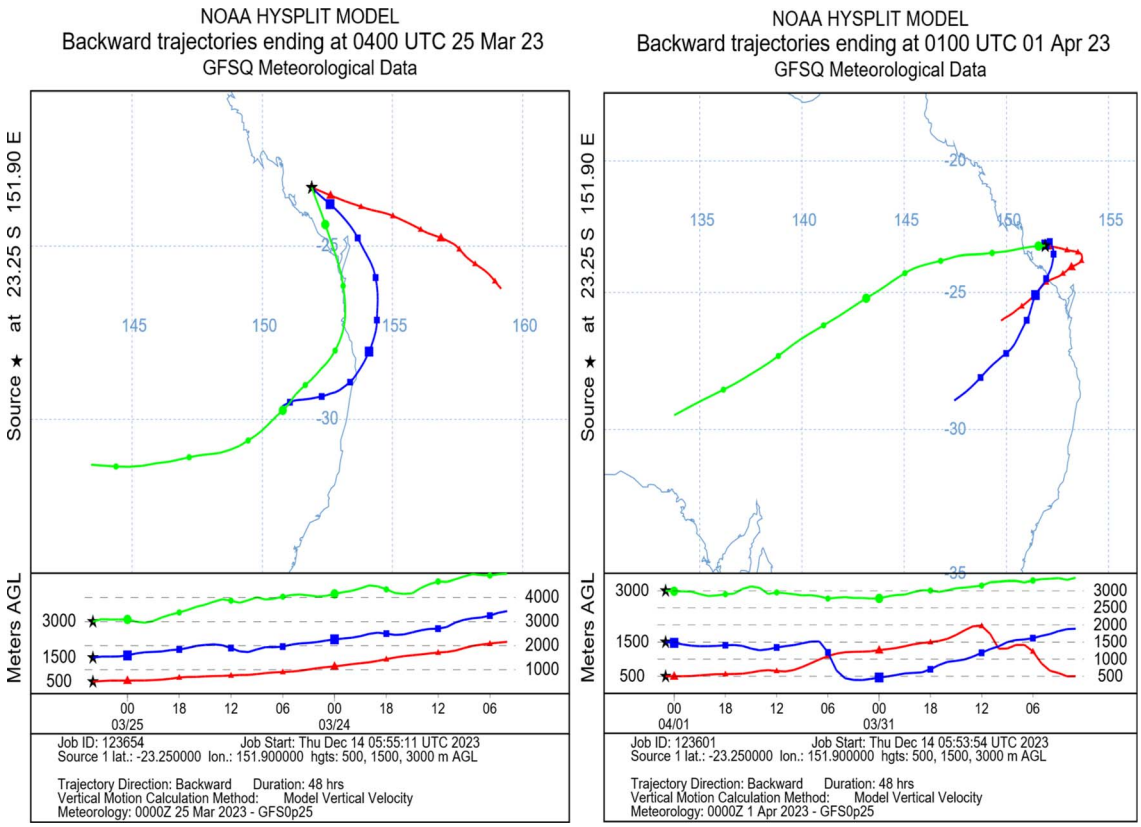

Fig. 4 48 hours back trajectories retrieved from the NOAA'S HYSPLIT model[61,62] for the two flights over the Great Barrier Reef (25/03/2023 on the left and 01/04/2023 on the right). Trajectories are shown according to height levels 500 (red), 1500 (blue) and 3000 m AGL (green). The vertical motion calculation method implemented was the model vertical velocity in both cases.

the 25th of March 2023, with predominately clean air masses, while on the 01st of April 2023 continental air masses dominated the boundary layer (see Fig. 4). We used 72 h backward-trajectory analysis from NOAA's Hybrid Single-Particle Lagrangian Integrated Trajectory model (HYSPLIT) atmospheric model[61,62] to investigate the source of aerosol particles over the GBR.

Vertical profiles of temperature, relative humidity, water vapour mixing ratio and background particle number concentration collected during spiral ascents are shown in Fig. 5. Temperature observed during the 25th of March ranged from 25.88 °C at low levels, to 13.16 °C at 2400 m a.s.l. (above sea level). Relative humidity during this day ranged from 62% to 90%. During the 01st of April, the boundary layer temperature decreased from 25.02 °C at low levels, to 8.27 °C at 3000 m a.s.l. While the relative humidity fluctuated from 16 to 91%. The vertical profile of particle number concentration (Fig. 5) from the 25th of March shows low particle concentration (<500 cm^{-3}) characteristic of clean marine air, while on the 1st of April, particle concentrations were detected up to ~1500 cm^{-3} in the boundary layer due to the influence of continental air masses.

Fig. 6a and b shows the number of droplets (N_d) measured at different heights in warm clouds between March 25 and April 1, 2023, over GBR. The cloud water content (CWC) during the measurements is indicated by colours (see Section S3 in the ESI† for detailed calculations of cloud properties). The cloud bases were located at ~700 m a.s.l., with the ambient air temperature at about 21 °C. During March 25, clouds were mostly affected by marine air masses at lower levels (see the vertical profile of the Aerodynamic Particle Size Distribution (APSD) Fig. S3–S5 in the ESI†), and thus, droplet concentrations reaching ~200 cm^{-3} were measured at the cloud base, which is characteristic of clean clouds. On April 1, the N_d measured at cloud bases was larger than on March 25 by a factor of ~2–3 (see Fig. 4b). Furthermore, during this day, the measured N_d was greater above the cloud base than at the cloud base on several cloud passes, which is a strong indication of secondary activation of CCN particles into cloud droplets due to the long-range transport of particles from the continental region.

Fig. 6c shows the evolution of the measured cloud droplet effective radius (r_e) as a function of altitude within convective cumulus and considering the adiabatic fraction greater than 0.25 (*i.e.*, the measured CWC is greater than 25% of the adiabatic CWC). Given the cleaner conditions on March 25, the lower concentration of CCN leads to the formation of larger droplets close to the cloud base. The figure shows that rain is initiated (drizzle water content – DWC > 0.05 g m^{-3}) when the droplets become larger than about r_e > ~12 μm. The CIP images confirmed the presence of drizzle starting on this r_e threshold (see Fig. S6 and S7 in the ESI†). The initiation of rain for r_e ~ 12 μm is probably due to the presence of Giant CCNs in this maritime region. A similarly low value of r_e for rain initiation

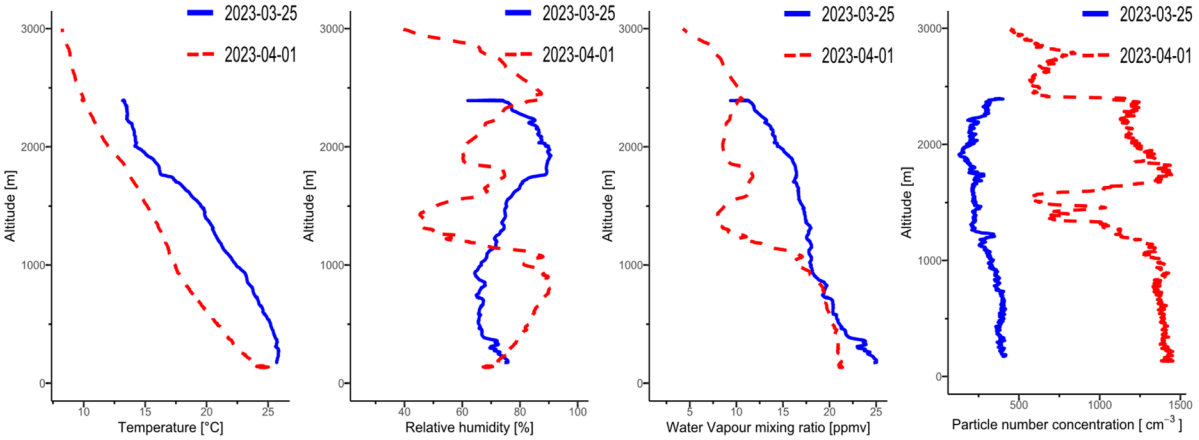

Fig. 5 Vertical profiles of temperature (°C), relative humidity (%), water vapour mixing ratio (ppmv) and background particle number concentration (cm^{-3}) collected during spiral ascents on the 25/03/2023 and 01/04/2023.

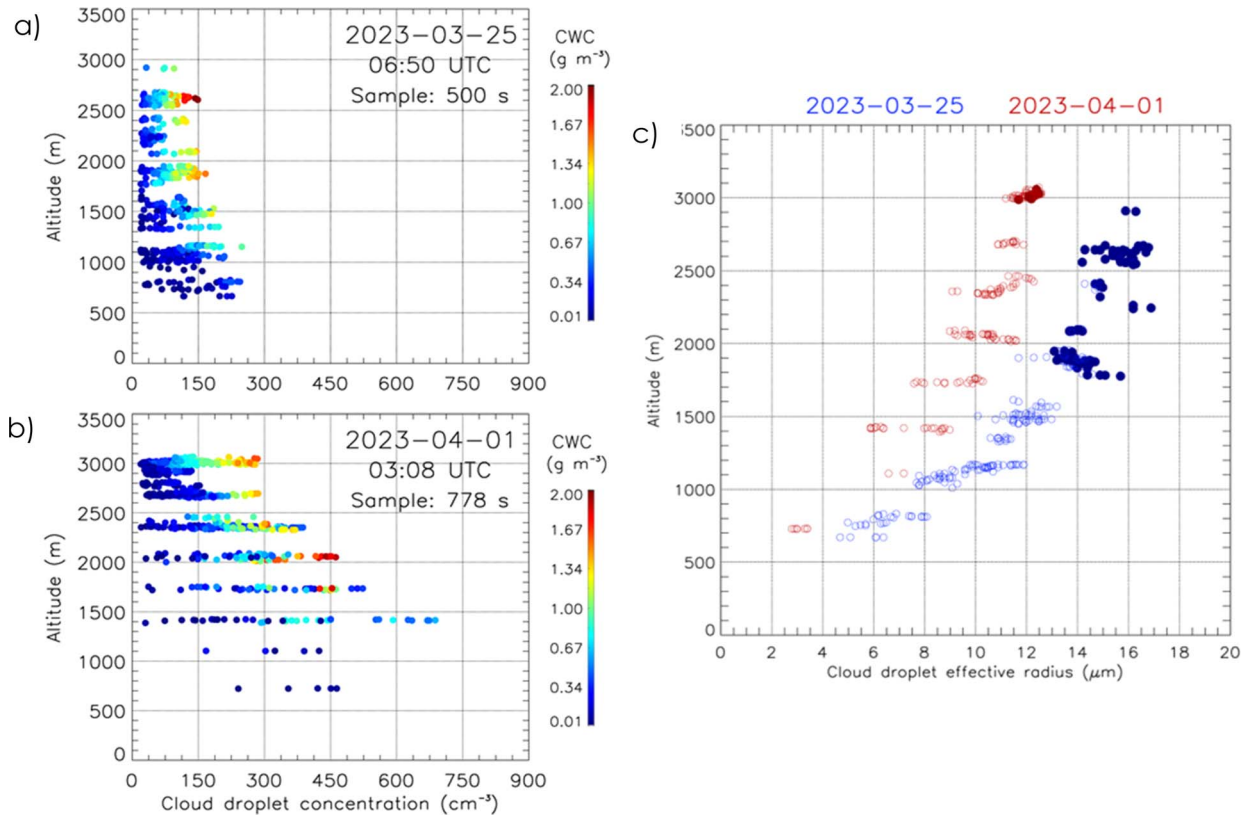

Fig. 6 (a and b) Vertical profiles of cloud droplet concentration (cm^{-3}) and cloud water content (g m^{-3}) for a background cloud with clean air mass in the boundary layer (2023-03-25) and a cloud with influence of continental air masses (2023-04-01). (c) Comparison of cloud droplet effective radius (μm) for a background cloud with clean air mass in the boundary layer (2023-03-25) and a cloud with influence of continental air masses (2023-04-01), calculated d = from CCP–CDP as a function of altitude. The filled points have drizzle water content >0.05 g m^{-3}.

over the ocean was observed by Braga *et al.*, 2017 (ref. 63) and Konwar *et al.*, 2012,[64] over the Atlantic Ocean and Indian Ocean, respectively. Due to the larger amount of N_d at cloud bases, the height of rain initiation for more polluted clouds measured on April 1 is higher than those measured on March 25.[63] The low CWC measured above the height of rain initiation indicates that most of it was already converted into raindrops.[65] For some cloud passes, the CWC and N_d measured above the height of rain initiation reach relatively higher values for similar altitudes, indicating new activation of particles.[66]

Summary

The new capabilities of the Cessna 337 Skymaster as a research aircraft were successfully tested over the Great Barrier Reef during the RRAP Cooling and Shading Campaign Mar–Apr

2023. The aims of the campaign included to perform *in situ* measurements of aerosols and clouds, meteorological conditions, and the sea-salt plumes generated for Marine Cloud Brightening testing. This manuscript described the capabilities of the new airborne platform (Cessna 337) and detailed the integrated instrumentation.

The new research aircraft proved to be a reliable platform to conduct measurements of marine warm clouds. We successfully combined the state-of-the-art meteorological, cloud microphysical, and aerosol instrumentation in a much smaller than typical research aircrafts used for studies of aerosol–cloud interactions.

The atmospheric aerosol and cloud data collected in different atmospheric conditions demonstrate the potential of the new airborne research platform. Data presented was obtained from precipitating cumulus clouds formed under clean and polluted conditions. We described the effect of long-range transport of continental and polluted air masses on the microphysical properties of warm clouds developed over the Reef. Our results suggest that air masses can transport the pollution produced on the east coast of Australia due to continental convective systems and atmospheric dynamics. Such additional particles promote the formation and development of relatively polluted clouds over the Reef. Furthermore, the aerosol particles (cloud condensation nuclei) from pollution dominate the concentrations around warm clouds, promoting secondary activation of droplets above cloud bases. Our results show that continentally sourced aerosols also suppress the collision and coalescence process in warm clouds and elevates the height of rain initiation. The practical result is the suppression of rain from warm clouds, as Rosenfeld *et al.* (2008)[67] documented for continental clouds over Australia.

Data availability

Data are available upon request from the authors.

Author contributions

Conceptualisation, DH-J, DR and DPH; writing—original draft, DH-J, DPH and RCB; writing—review and editing, DH-J, RCB, BK, and DPH; visualisation, DH-J and RCB; data collection, DH-J, CM, PB, AD, DR and DPH; data curation, RCB, CM, DH-J, and DPH; project administration and supervision, DPH; funding acquisition, DPH; resources; DPH. All authors have read and agreed to the published version of the manuscript.

Conflicts of interest

There are no conflicts to declare.

Acknowledgements

The Reef Restoration and Adaptation Program is funded by the partnership between the Australian Government's Reef Trust and the Great Barrier Reef Foundation. The authors would like to acknowledge the Traditional Owners of the Great Barrier Reef, particularly the Gooreng Gooreng, Gurang, Bailai, and Taribelang Bunda peoples, the traditional custodians of the area around Heron Reef for permission to undertake research in their traditional sea country. This research was conducted under a permit issued by the Great Barrier Reef Marine Park Authority (G19/43115.1). The authors acknowledge Eastern Air Services for their support in the fit out of the aircraft and during flight operations. The authors gratefully acknowledge the NOAA Air Resources Laboratory (ARL) for the provision of the HYSPLIT transport and dispersion model and/or READY website (**https://www.ready.noaa.gov**) used in this publication. Cloud type data (produced from Himawari-8) that was used in this paper' was supplied by the P-Tree System, Japan Aerospace Exploration Agency (JAXA).

References

1 S. J. Ghan and S. E. Schwartz, Aerosol Properties and Processes: A Path from Field and Laboratory Measurements to Global Climate Models, *Bull. Am. Meteorol. Soc.*, 2007, **88**(7), 1059–1084.
2 U. Lohmann and J. Feichter, Global indirect aerosol effects: a review, *Atmos. Chem. Phys.*, 2005, **5**, 715–737.
3 O. Boucher, D. Randall, P. Artaxo, C. Bretherton, G. Feingold, P. Forster, *et al.*, Clouds and Aerosols, in *Climate Change 2013 – The Physical Science Basis: Working Group I Contribution to the Fifth Assessment Report of the Intergovernmental Panel on Climate Change*, ed. Stocker T. F., Qin D., Plattner G.-K., Tignor M., Allen S. K., Doschung J., et al., Cambridge University Press, 2014. pp. 571–658.
4 B. Kravitz, A. Robock, O. Boucher, H. Schmidt, K. E. Taylor, G. Stenchikov, *et al.*, The Geoengineering Model Intercomparison Project (GeoMIP), *Atmos. Sci. Lett.*, 2011, **12**, 162–167.
5 B. Kravitz, P. M. Forster, A. Jones, A. Robock, K. Alterskjær, O. Boucher, *et al.*, Sea spray geoengineering experiments in the Geoengineering Model Intercomparison Project (GeoMIP): experimental design and preliminary results, *J. Geophys. Res.*, 2013, **118**, 11175–11186.
6 R. Wood, Assessing the potential efficacy of marine cloud brightening for cooling Earth using a simple heuristic model, *Atmos. Chem. Phys.*, 2021, **21**(19), 14507–14533.
7 J. Latham, K. Bower, T. Choularton, H. Coe, P. Connolly, G. Cooper, *et al.*, Marine cloud brightening, *Philos. Trans. R. Soc., A*, 2012, **370**, 4217–4262.
8 S. Twomey, Pollution and the planetary albedo, *Atmos. Environ.*, 1974, **8**, 1251–1256.
9 S. Twomey, The influence of pollution on the shortwave albedo of clouds, *Atmos. Sci.*, 1977, **34**, 1149–1152.
10 M. D. Zelinka, T. Andrews, P. M. Forster and K. E. Taylor, Quantifying components of aerosol-cloud-radiation interactions in climate models, *J. Geophys. Res.: Atmos.*, 2014, **119**, 7599–7615.
11 N. Bellouin, J. Quaas, E. Gryspeerdt, S. Kinne, P. Stier, D. Watson-Parris, *et al.*, Bounding Global Aerosol Radiative Forcing of Climate Change, *Rev. Geophys.*, 2019, **58**(1), e2019RG000660.

12 J. Latham, Control of global warming?, *Nature*, 1990, **347**, 339–340.
13 J. Latham, Amelioration of global warming by controlled enhancement of the albedo and longevity of low-level maritime clouds, *Atmos. Sci. Lett.*, 2002, 52–58.
14 J. Latham, P. Rasch, C.-C. Chen, L. Kettles, A. Gadian, A. Gettelman, *et al.*, Global temperature stabilization via controlled albedo enhancement of low-level maritime clouds, *Philos. Trans. R. Soc., A*, 2008, **366**, 3969–3987.
15 A. Jones, J. Haywood and O. Boucher, Climate impacts of geoengineering marine stratocumulus clouds, *J. Geophys. Res.: Atmos.*, 2009, **114**, D10106.
16 P. J. Rasch, J. Latham and C.-C. Chen, Geoengineering by cloud seeding: influence on sea ice and climate system, *Environ. Res. Lett.*, 2009, **4**, 045112.
17 K. Alterskjær, J. E. Kristjansson and Ø. Seland, Sensitivity to deliberate sea salt seeding of marine clouds – observations and model simulations, *Atmos. Chem. Phys. Discuss.*, 2011, **11**, 29527–29559.
18 K. Alterskjær and J. E. Kristjánsson, The sign of the radiative forcing from marine cloud brightening depends on both particle size and injection amount, *Geophys. Res. Lett.*, 2013, **40**, 210–215.
19 L. Ahlm, A. Jones, C. W. Stjern, H. Muri, B. Kravitz and J. E. Kristjánsson, Marine cloud brightening – as effective without clouds, *Atmos. Chem. Phys.*, 2017, **17**, 13071–13087.
20 C. W. Stjern, H. Muri, L. Ahlm, O. Boucher, J. N. S. Cole, D. Ji, *et al.*, Response to marine cloud brightening in a multi-model ensemble, *Atmos. Chem. Phys.*, 2018, **18**, 621–634.
21 J. Latham, A. Gadian, J. Fournier, B. Parkes, P. Wadhams and J. Chen, Marine cloud brightening: regional applications, *Philos. Trans. R. Soc., A*, 2014, **372**, 20140053.
22 J. Latham, J. Kleypas, R. Hauser, B. Parkes and A. Gadian, Can marine cloud brightening reduce coral bleaching?, *Atmos. Sci. Lett.*, 2013, **14**, 214–219.
23 D. Harrison, M. Baird, L. Harrison, S. Utembe, R. Schofield, R. E. Correa, *et al.*, *Reef Restoration and Adaptation Program: Environmental Modelling of Large Scale Solar Radiation Management. A Report provided to the Australian Government by the Reef Restoration and Adaptation Program*, 2019.
24 S. A. Condie, K. R. N. Anthony, R. C. Babcock, M. E. Baird 1, R. Beeden, C. S. Fletcher, *et al.*, Large-scale interventions may delay decline of the Great Barrier Reef, *R. Soc. Open Sci.*, 2021, **8**, 201296.
25 D. P. Harrison. An Overview of Environmental Engineering Methods for Reducing Coral Bleaching Stress, in *Oceanographic Processes of Coral Reefs Physical and Biological Links in The Great Barrier Reef*, ed. Wolanski E. and Kingsford M. J., Boca Raton, Fla, CRC Press, 2nd edn, 2024.
26 B. L. Spady, W. J. Skirving, G. Liu, J. L. De La Cour, C. J. McDonald and D. P. Manzello, Unprecedented early-summer heat stress and forecast of coral bleaching on the Great Barrier Reef, 2021-2022, *F1000Research*, 2022, **11**, 127.
27 O. Hoegh-Guldberg, Climate change, coral bleaching and the future of the world's coral reefs, *Mar. Freshwater Res.*, 1999, **50**, 839–866.
28 D. C. Hernandez-Jaramillo, L. Harrison, B. Kelaher, Z. Ristovski and D. P. Harrison, Evaporative Cooling Does Not Prevent Vertical Dispersion of Effervescent Seawater Aerosol for Brightening Clouds, *Environ. Sci. Technol.*, 2023, **57**(49), 20559–20570.
29 Z. Maalick, H. Korhonen, H. Kokkola, T. Kühn and S. Romakkaniemi, Modelling artificial sea salt emission in large eddy simulations, *Philos. Trans. R. Soc., A*, 2014, **372**, 20140051.
30 A. K. L. Jenkins and P. M. Forster, The inclusion of water with the injected aerosol reduces the simulated effectiveness of marine cloud brightening, *Atmos. Sci. Lett.*, 2013, **14**, 164–169.
31 G. Cooper, D. Johnston, J. Foster, L. Galbraith, A. Neukermans, R. Ormond, *et al.*, A review of some experimental spray methods for marine cloud brightening, *Int. J. Geosci.*, 2013, **4**, 78–97.
32 G. Cooper, J. Foster, L. Galbraith, S. Jain, A. Neukermans and B. Ormond, Preliminary results for salt aerosol production intended for marine cloud brightening, using effervescent spray atomization, *Philos. Trans. R. Soc., A*, 2014, **372**, 20140055.
33 A. Neukermans, G. Cooper, J. Foster, A. Gadian, L. Galbraith, S. Jain, *et al.*, Submicrometer salt aerosol production intended for marine cloud brightening, *Atmos. Res.*, 2014, **142**, 158–170.
34 J. Foster, G. Cooper, L. Galbrath, S. Jain, R. Ormond and A. Neukermans, Continuing Results for Effervescent Aerosol Salt Water Spray Nozzles Intended for Marine Cloud Brightening, *Int. J. Geosci.*, 2020, **11**, 563–589.
35 B. Stevens, F. Ament, S. Bony, S. Crewell, F. Ewald, S. Gross, *et al.*, A high-altitude long-range aircraft configured as a cloud observatory. The NARVAL Expeditions, *Bull. Am. Meteorol. Soc.*, 2019, 1061–1077.
36 K. K. Laursen, D. P. Jorgensen, G. P. Brasseur, S. L. Ustin and A. J. R. Huning, HIAPER: The new generation NSF/NCAR research aircraft, *Bull. Am. Meteorol. Soc.*, 2006, **87**(7), 896–910.
37 Z. Wang, J. French, V. Gabor, P. Wechsler, S. Haimov, A. Rodi, *et al.*, Single aircraft integration of remote sensing and in situ sampling for the study of cloud microphysics and dynamics, *Bull. Am. Meteorol. Soc.*, 2012, **93**(5), 653–668.
38 J. Ortega, J. R. Snider, J. N. Smith and J. M. Reeves, Comparison of aerosol measurement systems during the 2016 airborne ARISTO campaign, *Aerosol Sci. Technol.*, 2019, **53**, 871–885.
39 L. M. Russell, A. Sorooshian, J. H. Seinfeld, B. A. Albrecht, A. Nenes, L. Ahlm, *et al.*, Eastern Pacific Emitted Aerosol Cloud Experiment, *Bull. Am. Meteorol. Soc.*, 2013, **94**(5), 709–729.
40 R. Wood, C. R. Mechoso, C. S. Bretherton, R. A. Weller, B. Huebert, F. Straneo, *et al.*, The VAMOS Ocean-Cloud-Atmosphere-Land Study Regional Experiment (VOCALS-REx): goals, platforms, and field operations, *Atmos. Chem. Phys.*, 2011, **11**(2), 627–654.
41 M. Wendisch, U. Pöschl, M. O. Andreae, L. A. T. Machado, R. Albrecht, H. Schlager, *et al.*, ACRIDICON–CHUVA Campaign: Studying Tropical Deep Convective Clouds and

Precipitation over Amazonia Using the New German Research Aircraft HALO, *Bull. Am. Meteorol. Soc.*, 2016, **97**(10), 1885–1908.

42 D. Rosenfeld, W. L. Woodley, D. Axisa, E. Freud, J. G. Hudson and A. Givati, Aircraft measurements of the impacts of pollution aerosols on clouds and precipitation over the Sierra Nevada, *J. Geophys. Res.*, 2008, **113**, D15203.

43 S. M. Hvidegaard, R. Forsberg, H. Skourup, M. L. Kristensen, A. V. Olesen, A. F. Olesen, *et al.*, *ESA CryoVEx/KAREN Antarctica 2017-18 Final Report. Antarctic Field Campaign with Combined Airborne Ku/Ka-band Radar and Laser Altimeters, Together with Extensive in Situ Measurements over Sea- and Land Ice DTU Space*, National Space Institute, Technical University of Denmark, 2020, Contract No.: ISBN 978-87-91694-50-9.

44 H. M. Jones, G. Young, T. W. Choularton, K. N. Bower, T. Lachlan-Cope, S. O'Shea, *et al.*, Summertime Arctic Aircraft Measurements during ACCACIA, *Atmos. Chem. Phys.*, 2018, 1–40.

45 A. Brook and E. Ben-Dor, Supervised Vicarious Calibration (SVC) of Multi-Source Hyperspectral Remote-Sensing Data, *Remote Sens.*, 2015, **7**(5), 6196–6223.

46 J. A. Ogren, *Final Project Report – ARM CLASIC CIRPAS Twin Otter Aerosol*, NOAA ESRL/Global Monitoring Division, USDOE Office of Science (SC), United States, 2010.

47 R. Wood and T. P. Ackerman, Defining success and limits of field experiments to test geoengineering by marine cloud brightening, *Clim. Change*, 2013, **121**, 459–472.

48 M. S. Diamond, A. Gettelman, M. D. Lebsock, A. McComiskey, L. M. Russell, R. Wood, *et al. Opinion.*, To assess marine cloud brightening's technical feasibility, we need to know what to study—and when to stop, *Proc. Natl. Acad. Sci. U. S. A.*, 2022, **119**, e2118379119.

49 W. Junkermann and J. M. Hacker, Ultrafine particles over Eastern Australia: an airborne survey, *Tellus B*, 2015, **67**(1), 25308.

50 J. M. Hacker, D. Chen, M. Bai, C. Ewenz, W. Junkermann, W. Lieff, *et al.*, Using airborne technology to quantify and apportion emissions of CH4 and NH3 from feedlots, *Anim. Prod. Sci.*, 2016, **56**, 190–203.

51 M. Harley, I. Turner, M. Kinsela, J. H. Middleton, P. Mumford, K. Splinter, *et al.*, Extreme Coastal Erosion enhanced by anomalous extra-tropical storm wave direction, *Sci. Rep.*, 2017, **7**, 6033.

52 J. H. Middleton, C. G. Cooke, E. T. Kearney, P. J. Mumford, M. A. Mole, G. J. Nippard, *et al.*, Resolution and accuracy of an airborne scanning laser system for beach surveys, *J. Atmos. Oceanic Technol.*, 2013, **30**, 2452–2464.

53 E. Pendall, A. Hewitt, M. M. Boer, Y. Carrillo, N. F. Glenn, A. Griebel, *et al.*, Remarkable Resilience of Forest Structure and Biodiversity Following Fire in the Peri-Urban Bushland of Sydney, Australia, *Climate*, 2022, **10**, 86.

54 Y. Cai, D. Montague, W. Mooiweer-Bryan and T. Deshler, Performance characteristics of the ultra high sensitivity aerosol spectrometer for particles between 55 and 800 nm: Laboratory and field studies, *Aerosol Sci. Technol.*, 2008, 759–769.

55 R. H. Moore, E. B. Wiggins, A. T. Ahern, S. Zimmerman, L. Montgomery, P. C. Jost, *et al.*, Sizing response of the Ultra-High Sensitivity Aerosol Spectrometer (UHSAS) and Laser Aerosol Spectrometer (LAS) to changes in submicron aerosol composition and refractive index, *Atmos. Meas. Tech.*, 2021, **14**(6), 4517–4542.

56 J. R. Laing, D. A. Jaffe and A. J. Sedlacek, Comparison of Filter-based Absorption Measurements of Biomass Burning Aerosol and Background Aerosol at the Mt. Bachelor Observatory, *Aerosol Air Qual. Res.*, 2020, **20**(4), 663–678.

57 J. P. Marto, J. Zhangb and J. J. Schwaba, Plume analysis from field evaluations of a portable air quality monitoring system, *J. Air Waste Manage. Assoc.*, 2021, **71**(1), 70–80.

58 T. S. Bates, P. K. Quinn, J. E. Johnson, A. Corless, F. J. Brechtel, S. E. Stalin, *et al.*, Measurements of atmospheric aerosol vertical distributions above Svalbard, Norway, using unmanned aerial systems (UAS), *Atmos. Meas. Tech.*, 2013, **6**, 2115–2120.

59 D. Baumgardner, H. Jonsson, W. Dawson, D. O'Connor and R. Newton, The cloud, aerosol and precipitation spectrometer: a new instrument for cloud investigations, *Atmos. Res.*, 2001, **59–60**, 251–264.

60 W. D. King, D. A. Parkin and R. J. Handsworth, A Hot-Wire Liquid Water Device Having Fully Calculable Response Characteristics, *J. Appl. Meteorol. Climatol.*, 1978, **17**(12), 1809–1813.

61 A. F. Stein, R. R. Draxler, G. D. Rolph, B. J. B. Stunder, M. D. Cohen and F. Ngan, NOAA's HYSPLIT Atmospheric Transport and Dispersion Modeling System, *Bull. Am. Meteorol. Soc.*, 2015, **96**(12), 2059–2077.

62 G. Rolph, A. Stein and B. Stunder, Real-time Environmental Applications and Display sYstem: READY, *Environ. Model. Softw.*, 2017, **95**, 210–228.

63 R. C. Braga, D. Rosenfeld, R. Weigel, T. Jurkat, M. O. Andreae, M. Wendisch, *et al.*, Further evidence for CCN aerosol concentrations determining the height of warm rain and ice initiation in convective clouds over the Amazon basin, *Atmos. Chem. Phys.*, 2017, **17**(23), 14433–14456.

64 M. Konwar, R. S. Maheskumar, J. R. Kulkarni, E. Freud, B. N. Goswami and D. Rosenfeld, Aerosol control on depth of warm rain in convective clouds, *J. Geophys. Res.: Atmos.*, 2012, **17**(D13), 1–10.

65 R. C. Braga, D. Rosenfeld, O. O. Krüger, B. Ervens, B. A. Holanda, M. Wendisch, *et al.*, Linear relationship between effective radius and precipitation water content near the top of convective clouds: measurement results from ACRIDICON–CHUVA campaign, *Atmos. Chem. Phys.*, 2021, **21**(18), 14079–14088.

66 A. Efraim, O. Lauer, D. Rosenfeld, R. C. Braga, M. A. Franco, L. A. Kremper, *et al.*, Satellite-Based Detection of Secondary Droplet Activation in Convective Clouds, *J. Geophys. Res.: Atmos.*, 2022, **127**(12), e2022JD036519.

67 D. Rosenfeld, U. Lohmann, G. B. Raga, C. D. O'Dowd, M. Kulmala, S. Fuzzi, A. Reissell, *et al.*, Flood or drought: how do aerosols affect precipitation?, *Science*, 2008, **5**(5894), 1309–1313.